

**Sperlingite,  $(\text{H}_2\text{O})\text{K}(\text{Mn}^{2+}\text{Fe}^{3+})(\text{Al}_2\text{Ti})(\text{PO}_4)_4[\text{O}(\text{OH})][(\text{H}_2\text{O})_9(\text{OH})]\cdot 4\text{H}_2\text{O}$ , a new paulkerrite-group mineral, from the Hagendorf-Süd pegmatite, Oberpfalz, Bavaria, Germany.**

Christian Rewitzer<sup>1</sup>, Rupert Hochleitner<sup>2</sup>, Ian E. Grey<sup>3</sup>, Anthony R. Kampf<sup>4</sup>, Stephanie Boer<sup>5</sup>, Colin M. MacRae<sup>3</sup>, William G. Mumme<sup>3</sup>, Nicholas C. Wilson<sup>3</sup> and Cameron J. Davidson<sup>3</sup>.

<sup>1</sup>Independent researcher, Graf von Bogen Str. 6, D-93437 Furth im Wald, Germany.

<sup>2</sup>Mineralogical State Collection (SNSB), Theresienstrasse 41, 80333, München, Germany.

<sup>3</sup>CSIRO Mineral Resources, Private Bag 10, Clayton South, Victoria 3169, Australia.

<sup>4</sup>Mineral Sciences Department, Natural History Museum of Los Angeles County, 900 Exposition Boulevard, Los Angeles, CA 90007, USA.

<sup>5</sup>Australian Synchrotron, 800 Blackburn Road, Clayton, Victoria 3168, Australia.

Corresponding author: Ian E. Grey (email: [ian.grey@csiro.au](mailto:ian.grey@csiro.au))



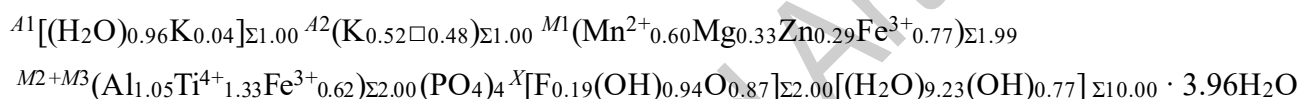
Mineralogical Society

This is a 'preproof' accepted article for Mineralogical Magazine. This version may be subject to change during the production process.

DOI: 10.1180/mgm.2024.40

## Abstract

Sperlingite,  $(\text{H}_2\text{O})\text{K}(\text{Mn}^{2+}\text{Fe}^{3+})(\text{Al}_2\text{Ti})(\text{PO}_4)_4(\text{O}(\text{OH}))[(\text{H}_2\text{O})_9(\text{OH})]\cdot 4\text{H}_2\text{O}$ , is a new monoclinic member of the paulkerrite group, from the Hagendorf-Süd pegmatite, Oberpfalz, Bavaria, Germany. It was found in corrosion pits of altered zwieselite, in association with columbite, hopeite, leucophosphite, mitridatite, scholzite, orange-brown zincoberaunite sprays and tiny green crystals of zincolibethenite. Sperlingite forms colourless prisms with pyramidal terminations, which are predominantly only 5 to 20  $\mu\text{m}$  in size, rarely to 60  $\mu\text{m}$  and frequently are multiply intergrown and are overgrown with smaller crystals. The crystals are flattened on  $\{010\}$  and slightly elongated along  $[100]$  with forms  $\{010\}$ ,  $\{001\}$  and  $\{111\}$ . Twinning occurs by rotation about  $c$ . The calculated density is  $2.40 \text{ g}\cdot\text{cm}^{-3}$ . Optically, sperlingite crystals are biaxial (+),  $\alpha = 1.600(\text{est})$ ,  $\beta = 1.615(5)$ ,  $\gamma = 1.635(5)$  (white light) and  $2V(\text{calc.}) = 82.7^\circ$ . The optical orientation is  $X = b$ ,  $Y = c$ ,  $Z = a$ . Neither dispersion nor pleochroism were observed. The empirical formula from electron microprobe analyses and structure refinement is



Sperlingite has monoclinic symmetry with space group  $P2_1/c$  and unit-cell parameters  $a = 10.428(2) \text{ \AA}$ ,  $b = 20.281(4) \text{ \AA}$ ,  $c = 12.223(2) \text{ \AA}$ ,  $\beta = 90.10(3)^\circ$ ,  $V = 2585.0(8) \text{ \AA}^3$  and  $Z = 4$ . The crystal structure was refined using synchrotron single-crystal data to  $wR_{\text{obs}} = 0.058$  for 5608 reflections with  $I > 3\sigma(I)$ . Sperlingite is the first paulkerrite-group mineral to have co-dominant divalent and trivalent cations at the  $M1$  sites; All other reported members have  $\text{Mn}^{2+}$  or  $\text{Mg}$  dominant at  $M1$ . Local charge balance for  $\text{Fe}^{3+}$  at  $M1$  is achieved by  $\text{H}_2\text{O} \rightarrow \text{OH}^-$  at  $\text{H}_2\text{O}$  coordinated to  $M1$ .

## 1. Introduction

Sperlingite was recently identified as a potential new mineral from scanning electron microscope and powder X-ray diffraction studies on a specimen collected at the Hagendorf Süd feldspar mine by Christian Rewitzer in 1974. The mine has been a prolific source of new minerals, particularly secondary phosphate minerals, both during its lifetime and after its closure and flooding in 1984, when studies were continued on specimens in extensive collections from the mine, including those of the lead author, Erich Keck (Birch et al., 2018) and Gabriella K. Robertson (Mills et al., 2016). Up to 1984, ten new minerals were published, including the phosphate minerals jungite, keckite, laueite, lehnerite, parascholzite, pseudolaueite, scholzite and wilhelmvierlingite as documented by Kastning and Schlüter (1994), while post-1984 another twenty three type specimens have been added. Of particular relevance to this study is the characterisation of the paulkerrite-group minerals pleysteinite (Grey et al., 2023a), hochleitnerite (Grey et al., 2023b), rewitzerite (Grey et al., 2023c) and fluor-rewitzerite (Hochleitner et al., 2024). Their formulae and unit-cell parameters are given in Table 1. Pleysteinite and hochleitnerite were originally reported to be isostructural with orthorhombic (*Pbca*) benyacarite (Demartin et al., 1993) based on laboratory-based sealed-tube single crystal diffraction studies. A more recent study, however, using microfocus synchrotron diffraction data (Rewitzer et al., 2024) has confirmed that they have monoclinic symmetry,  $P2_1/c$ , and are isostructural with rewitzerite and fluor-rewitzerite. Sperlingite also has monoclinic symmetry and is the fifth member of the group to be described from Hagendorf Süd. The mineral and its name have been approved by the International Mineralogical Association (IMA) Commission on New Minerals, Nomenclature and Classification (CNMNC), IMA-2023-120. The name honours Thomas Sperling (born 1963) for his contributions to Bavarian mineralogy, especially in phosphates from the pegmatite of Hühnerkobel in the Bavarian Forest (Schaaf et al., 2008). He is one of the best specialists in the history of Bavarian Mineralogy (Sperling, 2000). Mr. Sperling has agreed to the mineral being named after him. The holotype specimen is housed in the mineralogical collections of the Bavarian State Mineral Collection, Munich, registration number MSM38185. A cotype specimen used for the optical properties, powder XRD and Raman spectrum is located at the Natural History Museum of Los Angeles County, catalogue number 76310.

## 2. Occurrence and associated minerals

The lead author (CR) found the specimen CR202, containing sperlingite, in mid-1974 on the mine dump at the Hagendorf Süd feldspar mine, in the Oberpfalz, northeast Bavaria, Germany (49°39'1"N, 12°27'35"E). Based on the time of collection, and the mineral associations in the specimen, particularly zinc-bearing minerals, the specimen most likely originated from the 67 m level of the mine (Mücke, 1981; Grey et al., 2018). The matrix of the specimen consists of strongly corroded zwieselite residues in quartz, with clusters of sperlingite crystals occupying corrosion pits in the

zwieselite (Figure 1). Accompanying minerals are scholzite, hopeite, leucophosphite, orange-brown zincoberaunite sprays (Figure 2), tiny green crystals of zincolibethenite,  $\text{CuZn}(\text{PO}_4)(\text{OH})$ , olive green mitridatite and columbite. The colourless sperlingite crystals are commonly stained with mitridatite coatings (Figures 1 and 2). In addition to the close association of sperlingite with zwieselite, crystals are also observed growing on and within scholzite (Figure 3). Sperlingite and scholzite are likely the youngest phosphate minerals in the specimen.

### 3. Physical and optical properties

Crystals of sperlingite, in the form of colourless prisms with pyramidal terminations are predominantly only 5 to 20  $\mu\text{m}$  in size (Figure 3), rarely to 60  $\mu\text{m}$  and frequently are multiply intergrown and are overgrown with smaller crystals. The calculated density is  $2.40 \text{ g}\cdot\text{cm}^{-3}$  for the empirical formula and single-crystal unit-cell parameters.

The small size of the sperlingite crystals limited the measurement of the optical properties; however, it was possible to measure two indices of refraction in grain mounts. Based upon these and by comparison with the optical properties and morphologies of other paulkerrite group minerals, it was possible to conjecture the following properties: Biaxial (+),  $\alpha = 1.600(\text{est})$ ,  $\beta = 1.615(5)$ ,  $\gamma = 1.635(5)$  (white light) and  $2V(\text{calc.}) = 82.7^\circ$ . The optical orientation is  $X = b$ ,  $Y = c$ ,  $Z = a$ . Neither dispersion nor pleochroism were observed.

### 4. Raman spectroscopy

Raman spectroscopy was conducted on a Horiba XploRA PLUS spectrometer using a 532 nm diode laser, 100  $\mu\text{m}$  slit and 1800 gr/mm diffraction grating and a 100 $\times$  (0.9 NA) objective. The spectrum is shown in Figure 4. The O-H stretch region has a broad double hump that can be assigned to H-bonded water, with maxima at 3338 and 3057  $\text{cm}^{-1}$ . According to Libowitzsky (1999) these correspond to O..O distances involved in H-bonding of 2.65 and 2.75, corresponding to moderately strong H-bonding. Hydroxyl ion stretching is evident by a weak peak at 3600  $\text{cm}^{-1}$ . The H-O-H bending mode region for water has a peak at 1630  $\text{cm}^{-1}$ . Two peaks at 1012 and 965  $\text{cm}^{-1}$  in the P-O stretching region can be assigned to symmetric stretching modes while weaker peaks at 1135 and 1100  $\text{cm}^{-1}$  correspond to antisymmetric P-O stretching modes. Bending mode vibrations of the  $(\text{PO}_4)^{3-}$  groups are located at 610  $\text{cm}^{-1}$  and at 485 and 425  $\text{cm}^{-1}$ . Peaks at lower wavenumbers are related to lattice vibrations. The spectrum for sperlingite is dominated by a strong peak at 838  $\text{cm}^{-1}$  with a shoulder at 785  $\text{cm}^{-1}$ . These peaks are present in all paulkerrite-group minerals (Grey et al., 2023a-c) and can be assigned to Ti-O stretch vibrations for short Ti-O bonds that occur in linear trimers of corner-connected octahedra  $M2-M3-M2$  in the structure, by analogy with published Raman spectra for titanates containing short Ti-O distances (Tu et al., 1996; Bamberger et al., 1990; Silva et al., 2018).

## 5. Chemical composition

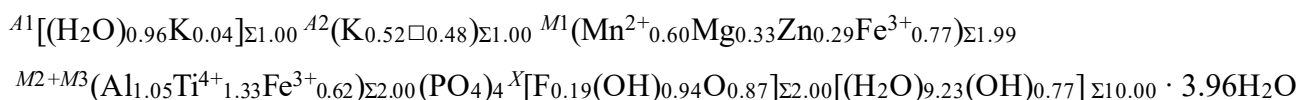
Highly hydrated paulkerrite-group minerals present problems for analysis because of dehydration in the high vacuum of the conductive film coater and the microprobe, resulting in severe cracking and high analysis totals (Sejkora *et al.*, 2006). Cracking of crystals of sperlingite during coating of a conductive iridium film is seen in the polished section used for the EMP analyses in Figure 3. To prevent further dehydration during analysis a cold stage cooled to liquid nitrogen temperature was employed in the microprobe and the specimen was precooled under dry nitrogen prior to introduction to the microprobe vacuum.

Crystals of sperlingite were analysed using wavelength-dispersive electron microprobe (EMP) spectrometry on a JEOL JXA 8530F Hyperprobe operated at an accelerating voltage of 15 kV and a beam current of 2.0 nA. The beam was defocused to typically ~5 µm. Both specimen and standards were coated with a 25 Å thick film of iridium for the analyses. The F K peak was partially overlapped by Mn L and Fe L and this was corrected using a peak overlap procedure. In addition the thin film correction procedure was utilized in STRATA (Pouchou 1993) to remove the effects of the Ir coating. There was insufficient material for direct determination of H<sub>2</sub>O, so it was calculated based on the ideal formula (14 H<sub>2</sub>O + 2OH- per 4 P). Analytical results (average of 11 analyses on 11 crystals) are given in Table 2, where they are compared with the published analyses for rewitzerite (Grey *et al.*, 2023c). Relatively high standard deviations (SD) are due to chemical zoning of the crystals, shown by variations in back-scatter contrast in Figure 3. The EMP results show strong positive correlations of Al with F ( $R^2 = 0.83$ ) and with K ( $R^2 = 0.78$ ) and negative correlations of Ti with K ( $R^2 = 0.86$ ) and with F ( $R^2 = 0.73$ ). Al correlates negatively with Fe ( $R^2 = 0.76$ ). (Mg+Zn) has a moderate negative correlation with Fe ( $R^2 = 0.61$ ).

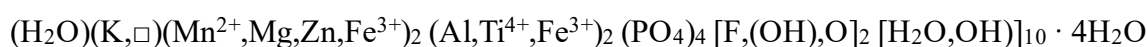
From the mean analyses, the number of atoms per formula unit (*apfu*), normalised to 4P *apfu* is:



Expressing the *apfu* in structural form and allowing for local charge balance for Fe<sup>3+</sup> at *M1*, by replacing an equivalent amount of H<sub>2</sub>O coordinated to *M1* with OH<sup>-</sup>, according to the model proposed for sigloite by Hawthorne (1988) gives the following empirical formula. The *M2* and *M3* sites are grouped based on the site-total-charge procedure (Bosi *et al.*, 2019a,b,; Grey *et al.* 2023d):



The simplified formula is



The ideal formula is (H<sub>2</sub>O)K(Mn<sup>2+</sup>Fe<sup>3+</sup>)(Al<sub>2</sub>Ti)(PO<sub>4</sub>)<sub>4</sub>[O(OH)][(H<sub>2</sub>O)<sub>9</sub>(OH)]·4H<sub>2</sub>O, which requires K<sub>2</sub>O 5.04, MnO 7.60, Al<sub>2</sub>O<sub>3</sub> 10.92, P<sub>2</sub>O<sub>5</sub> 30.41, TiO<sub>2</sub> 8.56, Fe<sub>2</sub>O<sub>3</sub> 8.55, H<sub>2</sub>O 28.92, total 100.00 wt%.

Note that the  $M1$  site has similar levels of divalent (1.22 *apfu*) and trivalent (0.77 *apfu*) cations, and the dominant divalent cation is  $Mn^{2+}$ , giving the end-member  $M1$  ( $=M1a+M1b$ ) site composition as ( $Mn^{2+}Fe^{3+}$ ), illustrated in Figure 5, while the merged ( $M2_2M3$ ) site composition corresponds to the end-member composition ( $Al_2Ti$ ) as shown in Figure 6.

## 6. Crystallography

X-ray powder diffraction data were obtained using a Rigaku R-Axis Rapid II curved imaging plate microdiffractometer, with monochromatized  $MoK\alpha$  radiation. Observed  $d$  values and intensities were derived by profile fitting using JADE Pro software. Data (in Å for  $MoK\alpha$ ) are given in Table 3. Refined monoclinic (space Group:  $P2_1/c$  (#14)) unit cell parameters from the powder data using JADE Pro with whole pattern fitting are  $a = 10.43(3)$  Å,  $b = 20.28(3)$  Å,  $c = 12.22(3)$  Å,  $\beta = 90.1(6)^\circ$ ,  $V = 2585(10)$  Å<sup>3</sup> and  $Z = 4$ .

A crystal measuring 0.020 x 0.020 x 0.010 mm was used for a data collection at the Australian Synchrotron microfocus beamline MX2 (Aragao et al., 2018). Intensity data were collected using a Dectris Eiger 16M detector and monochromatic radiation with a wavelength of 0.7109 Å. The crystal was maintained at 100 K in an open-flow nitrogen cryostream during data collections. The diffraction data were collected using a single 36 second sweep of 360° rotation around phi. The resulting dataset consists of 3600 individual images with an approximate phi angle of each image being 0.1 degrees. The raw intensity dataset was processed using XDS software (Kabsch, 2010) to produce data files that were analysed using SHELXT (Sheldrick, 2015) and JANA2006 (Petříček et al., 2014). Refined unit-cell parameters and other data collection conditions are given in Table 4.

### 6.1 Structure refinement

A structural model for sperlingite was obtained in space group  $P2_1/c$  using SHELXT (Sheldrick, 2015). The SHELXT model had the same structure as for rewitzerite (Grey et al., 2023c) and so the rewitzerite coordinate file was used to initiate the refinement to ensure the same atom labelling. Twinning was implemented with 2-fold rotation about  $c$ . To establish site scattering at the  $M1$  to  $M3$  sites, pairs of light and heavy elements were incorporated at the sites and their occupancies were refined;  $Mn+Mg$  at  $M1$  and  $Ti+Al$  at  $M2$  and  $M3$ . Initially K plus O (for  $H_2O$ ) were incorporated at the  $A$  sites with full occupancy, but refinement of their relative amounts gave a K content considerably lower than the EMP value. Next, vacancies were introduced to increase the K content, but with 3 components at the  $A$  sites, the site compositions are indeterminate. The simplest model, with only two components at each site, was to have K plus vacancies at the site with the higher scattering, and  $H_2O$  plus K at the other. This gave 0.66 K *apfu*, which is within the range of

EMP analyses for K. After preliminary refinements, the program OccQP (Wright et al., 2000) was applied to optimise the site occupancies based on the empirical formula together with refined bond distances and site scattering. The output from OccQP had only Al and Ti at the *M3* sites, but Al, Ti and Fe at the *M2* sites. The *M2* site occupancies were then modified to include a fixed amount of Fe (0.31 Fe per site) with refinement of Al and Ti. A pleasing result from this refinement was that the total Al and Ti contents from refinement of the occupancies at the *M2* and *M3* sites agreed with the values from the EMP analyses.

Refinement with anisotropic displacement parameters in JANA2006 converged at  $R_{obs} = 0.050$  for 5608 reflections with  $I > 3\sigma(I)$ . Difference Fourier maps were used to search for H atoms but unambiguous locations could not be established. This is most likely because the chemical zoning caused local atomic shifts of the oxygen atoms in response to different elements at metal atom sites, which is reflected in high atomic displacement parameters as shown in Table 5. Details of the data collection and refinement are given in Table 4. The refined coordinates, equivalent isotropic displacement parameters and bond valence sum (BVS) values (Gagné and Hawthorne, 2015) are reported in Table 5. For the *M1* sites, the BVS values were calculated based on the site occupancy in the empirical formula,  $0.30\text{Mn}^{2+}+0.165\text{Mg}+0.145\text{Zn}+0.39\text{Fe}^{3+}$ . For the *M2*, *M3* and *A* sites the BVS values were calculated using the refined site occupancies as listed in Table 6. Selected interatomic distances are reported in Table 7.

Although the H atoms in sperlingite could not be located during the refinement, we have located the majority of H atoms in refinements of the isostructural minerals fluor-rewitzerite (Hochleitner et al., 2024) and macraeite (Grey et al. 2024) and have established the H-bonding in these paulkerrite-group minerals. There is good agreement between the H-bonding schemes for the two minerals and also with that reported for benyacarite (Demartin et al., 1993). Applying this information to sperlingite, the O...O pairs involved in hydrogen bonding are listed in Table 8, together with bond valences,  $s$ , calculated from O..O using the Ferraris and Ivaldi (1988) formula  $s = [(O..O)/2.17]^{-8.2} + 0.06$ . The contributions to the BVS from the H bonds, as listed in Table 8, complement reasonably the undersaturated BVS values for the acceptor anions, O1 to O8, in Table 5.

TTT T

## T6.2 Description of structure

The crystal structure for sperlingite is based on an open 3D framework of corner-connected octahedra and tetrahedra of composition  $[(\text{MnFe}^{3+})(\text{Al}_2\text{Ti})(\text{PO}_4)_4\text{O}_2(\text{H}_2\text{O})_{10}]^{1-}$ , with water molecules and  $\text{K}^+$  ions occupying  $\langle 110 \rangle$  channels in the framework. Although H atoms were not located in the refinement the BVS values in Table 5 show that O9 to O15 are  $\text{H}_2\text{O}$ , as well as the main constituent at *A1*. The groups O9 to O12 are coordinated to *M1* and O13 is coordinated to *M2*. The framework is

built from heteropolyhedral layers parallel to (001) and located at  $z = \frac{1}{4}$  and  $\frac{3}{4}$ , shown in Figure 7, that are interconnected by corner-sharing of  $M2O_4X(H_2O)$  octahedra with  $M3O_4X_2$  octahedra located at  $z = 0$  and  $\frac{1}{2}$ . The heteropolyhedral (001) layers are built from [100] kröhnkite-type chains (Hawthorne, 1985) of 4-member rings of corner-connected  $PO_4$  tetrahedra and  $M2O_4X(H_2O)$  octahedra. Each  $PO_4$  tetrahedron also shares a corner with  $M1O_2(H_2O)_4$  octahedra along [010]. The corner-shared linkages form 8-member rings of alternating octahedra and tetrahedra. The  $A1$  ( $H_2O$ ) and  $A2$  (K) sites are located in the 8-member rings as shown in Figure 7.

The major difference between the crystal structure of sperlingite and that of orthorhombic paulkerrite-group minerals such as benyacarite (Demartin *et al.*, 1993) is an ordering of  $H_2O$  and K at the  $A1$  and  $A2$  sites, whereas they are disordered at a single  $A$  site in benyacarite. The different coordination environments at  $A1$  and  $A2$  are compared in Table 7 and shown in Figure 7. The coordinations are very similar, except for the bond to O15, with the K-containing  $A2$  site having a distance to O15a that is 0.24 Å shorter than the  $A1$ -O15b distance. The same large difference in  $A$ -O15 distances is observed for other monoclinic paulkerrite-group minerals, rewitzerite (Grey *et al.*, 2023c) and paulkerrite (Grey *et al.*, 2023d).

## 7. Discussion

The general formula for monoclinic paulkerrite-group minerals is

$A1A2M1_2M2_2M3(PO_4)_4X_2(H_2O)_{10} \cdot 4H_2O$ . Sperlingite is the first paulkerrite-group mineral to have a co-dominant trivalent cation at the  $M1$  sites. All previous members of the group have had either Mg or  $Mn^{2+}$  as the dominant cation at  $M1$ . The evidence for trivalent  $Fe^{3+}$  in sperlingite is indirect as there was insufficient material available for a direct determination of the valence state.

Nevertheless, the bond distances and BVS values give strong support for trivalent Fe at  $M1$ . Using the Shannon (1976) ionic radii for 6-coordinated cations and 2-coordinated  $O^{2-}$  gives, for the proposed site occupations in the empirical formula  $(Mn^{2+}_{0.30}Mg_{0.165}Zn_{0.145}Fe^{n+}_{0.39})$ ,  $\langle M1-O \rangle = 2.077$  Å for Fe as  $Fe^{3+}$  and 2.149 Å for  $Fe^{2+}$ . These compare with the  $\langle M1a-O \rangle$  and  $\langle M1b-O \rangle$  values obtained from the refinement of 2.079 and 2.087 Å. Thus, the refined bond distances for the  $M1$  sites give good indirect support to the site being occupied by a mix of large  $Mn^{2+}$  and small  $Fe^{3+}$ , together with minor Mg and Zn.

In all previous studies on paulkerrite-group minerals, valency variations occur only at the  $A$  sites ( $K^+$ ,  $H_2O$ , vacancy), and the  $M2$  and  $M3$  sites ( $Fe^{3+}$ ,  $Al^{3+}$ ,  $Ti^{4+}$ ). The species at all three sites coordinate to anions at the  $X$  sites, and so the charge balance in the structure can be maintained by variations in the ratio of univalent ( $F^-$ ,  $OH^-$ ) to divalent ( $O^{2-}$ ) anions at  $X$ . Cations at the  $M1$  site do not coordinate to anions at  $X$ , and so for sperlingite, with a mix of divalent and trivalent cations at  $M1$ , a different local charge balance mechanism is required. We have used the mechanism proposed



by Hawthorne (1988) for sigloite,  $\text{Fe}^{3+}[(\text{H}_2\text{O})_3\text{OH}][\text{Al}_2(\text{PO}_4)_2(\text{OH})_2(\text{H}_2\text{O})_2] \cdot 2\text{H}_2\text{O}$ , the oxidised analogue of paravauxite,  $\text{Fe}^{2+}(\text{H}_2\text{O})_4[\text{Al}_2(\text{PO}_4)_2(\text{OH})_2(\text{H}_2\text{O})_2] \cdot 2\text{H}_2\text{O}$ . These laueite-group minerals have a  $\text{MO}_2(\text{H}_2\text{O})_4$  octahedron that is topologically identical to the  $M1$ -centred octahedra in sperlingite, and which is occupied by  $\text{Fe}^{2+}$  in paravauxite. When the Fe is oxidized to  $\text{Fe}^{3+}$  as in sigloite, local charge balance is retained by replacement of  $\text{H}_2\text{O}$  that is coordinated to  $M$  by  $\text{OH}^-$ . Applying this mechanism to sperlingite gives local charge balance when  $\text{Fe}^{3+}$  is present at the  $M1$  site, by partial replacement of  $\text{H}_2\text{O}$  by  $\text{OH}^-$  at the octahedron. The four  $\text{H}_2\text{O}$  groups coordinating to  $M1$  are O9 to O12, inclusive. As seen from Tables 5 and 7, the bond distances and BVS values are similar for the four coordinated  $M1$ - $\text{H}_2\text{O}$  at both  $M1a$  and  $M1b$  sites suggesting that the  $\text{OH}^-$  replacement for  $\text{H}_2\text{O}$  is disordered over the four  $\text{H}_2\text{O}$  groups per octahedron.

Taking into account the mixed valence cations at  $M1$  and the  $\text{OH}^-$  for  $\text{H}_2\text{O}$  substitution, the resulting ideal formula for sperlingite is  $(\text{H}_2\text{O})\text{K}(\text{Mn}^{2+}\text{Fe}^{3+})(\text{Al}_2\text{Ti})(\text{PO}_4)_4(\text{O}(\text{OH}))[(\text{H}_2\text{O})_9(\text{OH})] \cdot 4\text{H}_2\text{O}$ . The general formula for monoclinic paulkerrite group minerals needs a revision to account for minerals like sperlingite, giving  $A1A2(M1^{3+n}M1^{2+2-n})M2_2M3(\text{PO}_4)_4X_2(\text{H}_2\text{O})_{10-n}(\text{OH})_n \cdot 4\text{H}_2\text{O}$ . Paulkerrite-group minerals described to date have  $n = 0$ , while sperlingite has  $n = 1$ .

Sperlingite is chemically and structurally most closely related to rewitzerite (Grey et al, 2023c) with the same dominant  $A$ ,  $(M2_2M3)$  and  $X$  species. The properties of the two minerals are compared in Table 9. The properties of the two minerals are compared in table 8. mineral with only trivalent cations at  $M1$  has

## Acknowledgments

This research was undertaken in part using the MX2 beamline at the Australian Synchrotron, part of ANSTO, and made use of the Australian Cancer Research detector.

## References

- Aragao, D., Aishima, J., Cherukuvada, H., Clarken, R., Clift, M., Cowieson, N.P., Ericsson, D.J., Gee, C.L., Macedo, S., Mudie, N., Panjekar, S., Price, J.R., Riboldi-Tunncliffe, A., Rostan, R., Williamson, R. and Caradoc-Davies, T.T. (2018) MX2: a high-flux undulator microfocus beamline serving both the chemical and macromolecular crystallography communities at the Australian Synchrotron, *Journal of Synchrotron Radiation*, **25**, 885–891.
- Bamberger, C.E., Begun, G.M. and MacDougall, C.S. (1990) Raman spectroscopy of potassium titanates: Their synthesis, hydrolytic reactions and thermal stability. *Applied Spectroscopy*, **44**, 31–37.
- Birch, W.D., Grey, I.E., Keck, E., Mills, S.J. and Mumme, W.G. (2018) The Hagendorf Süd pegmatite: Australian-Bavarian collaboration on the characterization of new secondary phosphate minerals. *Australian Journal of Mineralogy*, **19**, 7–19.
- Bosi, F., Hatert, F., Halenius, U., Pasero, M., Ritsuro, M. and Mills, S.J. (2019a) On the application of the IMA-CNMNC dominant-valency rule to complex mineral compositions. *Mineralogical Magazine*, **83**, 627–632.
- Bosi F., Biagioni C. and Oberti R. (2019b) On the chemical identification and classification of minerals. *Minerals*, **9**, 591.
- Demartin, F., Pilati, T., Gay, H.D. and Gramaccioli, C.M. (1993) The crystal structure of a mineral related to paulkerrite. *Zeitschrift für Kristallographie*, **208**, 57–71.
- Demartin, F., Gay, H.D. Gramaccioli, C.M. and Pilati, T. (1997) Benyacarite, a new titanium-bearing phosphate mineral species from Cerro Blanco, Argentina. *The Canadian Mineralogist*, **35**, 707–712.
- Ferraris, G. and Ivaldi, G. (1988) Bond valence vs. bond length in O...O hydrogen bonds. *Acta Crystallographica*, **B44**, 341–344.
- Fransolet, A.-M., Oustriere, P., Fontan, F. and Pillard, F. (1984) La mantienneite, une nouvelle espece minerale du gisement de vivianite d'Anloua, Cameroun. *Bulletin de Mineralogie*, **107**, 737–744.
- Gagné, O.C. and Hawthorne, F.C. (2015) Comprehensive derivation of bond-valence parameters for ion pairs involving oxygen. *Acta Crystallographica*, **B71**, 562–578.
- Grey, I.E., Keck, E., MacRae, C.M., Glenn, A.M., Mumme, W.G., Kampf, A.R. and Cashion, J.D. (2018) Secondary Zn-bearing phosphate minerals associated with alteration of phosphophyllite at Hagendorf-Süd, Bavaria. *Eur. J. Mineral.*, **30**, 1007–1020.
- Grey, I.E., Hochleitner, R., Rewitzer, C., Kampf, A.R., MacRae, C.M., Gable, R.W., Mumme, W.G., Keck, E. and Davidson, C. (2023a) Pleysteinite,  $[(\text{H}_2\text{O})_{0.5}\text{K}_{0.5}]_2\text{Mn}_2\text{Al}_3(\text{PO}_4)_4\text{F}_2(\text{H}_2\text{O})_{10}\cdot 4\text{H}_2\text{O}$ , the Al analogue of benyacarite, from the Hagendorf Süd pegmatite, Oberpfalz, Bavaria, Germany. *European Journal of Mineralogy*, **35**, 189–197.

- Grey, I. E., Keck, E., Kampf, A. R., MacRae, C. M., Gable, R. W., Mumme, W. G., Glenn, A. M., and Davidson, C. (2023b) Hochleitnerite,  $[\text{K}(\text{H}_2\text{O})]\text{Mn}_2(\text{Ti}_2\text{Fe})(\text{PO}_4)_4\text{O}_2(\text{H}_2\text{O})_{10}\cdot 4\text{H}_2\text{O}$ , a new paulkerrite-group mineral, from the Hagendorf-Süd pegmatite, Oberpfalz, Bavaria, Germany. *European Journal of Mineralogy*, **35**, 635–643.
- Grey, I.E., Hochleitner, R., Kampf, A.R., Boer, S., MacRae, C.M., Mumme, W.G., and Keck, E. (2023c) Rewitzerite,  $\text{K}(\text{H}_2\text{O})\text{Mn}_2(\text{Al}_2\text{Ti})(\text{PO}_4)_4[\text{O}(\text{OH})](\text{H}_2\text{O})_{10}\cdot 4\text{H}_2\text{O}$ , a new monoclinic paulkerrite-group mineral, from the Hagendorf Süd pegmatite, Oberpfalz, Bavaria, Germany. *Mineralogical Magazine*, **87**, 830–838.
- Grey, I.E., Boer, S., MacRae, C.M., Wilson, N.C., Mumme, W.G. and Bosi, F. (2023d) Crystal chemistry of type paulkerrite and establishment of the paulkerrite group nomenclature. *European Journal of Mineralogy*, **35**, 909–919.
- Grey, I.E., Rewitzer, C., Hochleitner, Kampf, A.R., Boer, S., Mumme, W.G.. and Wilson, N.C. (2024) Macraeite,  $[(\text{H}_2\text{O})\text{K}]\text{Mn}_2(\text{Fe}_2\text{Ti})(\text{PO}_4)_4[\text{O}(\text{OH})](\text{H}_2\text{O})_{10}\cdot 4\text{H}_2\text{O}$ , a new monoclinic paulkerrite-group mineral from the Cubos-Mesquitela-Mangualde pegmatite, Portugal, *European Journal of Mineralogy*, **36**, 267–278.
- Hawthorne, F.C. (1985) Towards a structural classification of minerals: The  ${}^{\text{vi}}\text{M}^{\text{iv}}\text{T}_2\Phi_n$  minerals. *American Mineralogist*, **70**, 455–473.
- Hawthorne, F.C. (1988) Sigloite: The oxidation mechanism in  $[\text{M}^{3+}_2(\text{PO}_4)_2(\text{OH})_2(\text{H}_2\text{O})_2]^{2-}$  structures. *Mineralogy and Petrology*, **38**, 201–211.
- Hochleitner, R., Grey, I.E., Kampf, A.R., Boer, S., MacRae, C.M., Mumme, W.G. and Wilson, N.C. (2024) Fluor-rewitzerite,  $[(\text{H}_2\text{O})\text{K}]\text{Mn}_2(\text{Al}_2\text{Ti})(\text{PO}_4)_4[\text{OF}](\text{H}_2\text{O})_{10}\cdot 4\text{H}_2\text{O}$ , a new paulkerrite-group mineral, from the Hagendorf Süd pegmatite, Oberpfalz, Bavaria, Germany. *European Journal of Mineralogy*, **36**. xxx-yyy.
- Kabsch, W. (2010) XDS. *Acta Crystallographica D* **66**, 125–132.
- Kastning, J. and Schlüter, J. (1994). Die Mineralien von Hagendorf und ihre Bestimmung. Schriften des Mineralogischen Museums der Universität Hamburg, Band 2, C. Weise Verlag, Munich, 95 pp.
- Libowitzky, E. (1999) Correlation of O-H stretching frequencies and O-H...O hydrogen bond lengths in minerals. *Monatsch. Chemie*, **130**, 1047–1059.
- Mills, S.J., Grey, I.E., Kampf, A.R., Birch, W.D., MacRae, C.M., Smith, J.B. and Keck, E. (2016) Kayrobertsonite,  $\text{MnAl}_2(\text{PO}_4)_2(\text{OH})_2\cdot 6\text{H}_2\text{O}$ , a new phosphate mineral related to nordgauite. *European Journal of Mineralogy*, **29**, 649–654.
- Mücke, A. (1981) The paragenesis of the phosphate minerals of the Hagendorf pegmatite — a general view, *Chemie der Erde*, **40**, 217–234.

- Peacor, D.R., Dunn, P.J. and Simmons, W.B. (1984) Paulkerrite a new titanium phosphate from Arizona. *The Mineralogical Record*, 1984, 303–306.
- Petříček, V., Dušek, M. and Palatinus, L. (2014) Crystallographic Computing System JANA2006: General features. *Zeitschrift für Kristallographie*, **229**, 345–352.
- Pouchou, J. L. (1993) X-ray microanalysis of stratified specimens. *Analytica Chimica Acta*, 283 (1), 81-97.
- Rewitzer, C., Hochleitner, R., Grey, I.E., MacRae, C.M., Mumme, W.G., Boer, S., Kampf, A.R. and Gable, R.W. (2024) Monoclinic pleysteinite and hochleitnerite from the Hagendorf Süd pegmatite. Synchrotron microfocus diffraction studies on paulkerrite-group minerals. *Canadian Journal of Mineralogy and Petrology*, **62**, xxx-yyy.
- Schaaf, P., Sperling, T. and Müller-Sohnius, D. (2008): Pegmatites from the Bavarian Forest, SE Germany: Geochronology, Geochemistry and Mineralogy. – *Geologica Bavarica*, **110**, 204-303 and 420—429.
- Sejkora, J., Skoda, R., Ondrus, P., Beran, P. and Susser, C. (2006) Mineralogy of phosphate accumulations in the Huber stock, Krasno ore district, Slavkovsky les area, Czech Republic, *J. Czech geol. Soc.*, **51**, 103–147.
- Shannon R.D. (1976) Revised effective ionic radii and systematic studies of interatomic distances in halides and chalcogenides. *Acta Crystallographica*, **A32**, 751–767.
- Sheldrick, G.M. (2015) Crystal-structure refinement with SHELX. *Acta Crystallographica*, **C71**, 3–8.
- Silva, F.L.R., Filho, A.A.A., Silva, M.B., Balzuweit, K., Bantiignies, J-L., Caetano, E.W.S., Moreira, R.L., Freire, V.N. and Righi, A. (2018) Polarized raman, FTIR, and DFT study of Na<sub>2</sub>Ti<sub>3</sub>O<sub>7</sub> microcrystals. *Journal of Raman Spectroscopy*, **49**, 535–548.
- Sperling, T. (2000) The geological mapping of Bavaria under the leadership of Carl Wilhelm von Gümbel. - Third congress on regional cartography and information systems (Munich, October 24th - 27th, 2000), Proceedings: 299-302; München.
- Tu, C.-S., Guo, A.R., Tao, R., Katiyar, R.S., Guo, R. and Bhalla, A.S. (1996) Temperature dependent Raman scattering in KTiOPO<sub>4</sub> and KTiOAsO<sub>4</sub> single crystals. *Journal of Applied Physics*, **79**, 3235–3240.
- Wright, S.E., Foley, J.A. and Hughes, J.M. (2000) Optimisation of site occupancies in minerals using quadratic programming. *American Mineralogist*, **85**, 524–531.

**Table 1.** Monoclinic ( $P2_1/c$ ) paulkerrite-group minerals from the Hagendorf-Süd pegmatite, Bavaria.

Pleysteinite (Rewitzer et al., 2024)	$[(\text{H}_2\text{O})\text{K}]\text{Mn}_2\text{Al}_3(\text{PO}_4)_4\text{F}_2(\text{H}_2\text{O})_{10}\cdot 4\text{H}_2\text{O}$ $a = 10.440(5), b = 20.588(5), c = 12.2341(3) \text{ \AA}$ $\beta = 90.38(1)^\circ$
Hochleitnerite (Rewitzer et al., 2024)	$[(\text{H}_2\text{O})\text{K}]\text{Mn}_2(\text{Ti}_2\text{Fe})(\text{PO}_4)_4\text{O}_2(\text{H}_2\text{O})_{10}\cdot 4\text{H}_2\text{O}$ $a = 10.547(2), b = 20.577(4), c = 12.373(2) \text{ \AA}$ $\beta = 90.09(3)^\circ$
Rewitzerite (Grey et al., 2023c)	$[\text{K}(\text{H}_2\text{O})]\text{Mn}_2(\text{Al}_2\text{Ti})(\text{PO}_4)_4[\text{O}(\text{OH})](\text{H}_2\text{O})_{10}\cdot 4\text{H}_2\text{O}$ $P2_1/c, a = 10.444(2), b = 20.445(2), c = 12.269(1) \text{ \AA}, \beta = 90.17(3)^\circ$
Fluor-rewitzerite (Hochleitner et al., 2024)	$[(\text{H}_2\text{O})\text{K}]\text{Mn}_2(\text{Al}_2\text{Ti})(\text{PO}_4)_4(\text{OF})(\text{H}_2\text{O})_{10}\cdot 4\text{H}_2\text{O}$ $a = 10.407(1), b = 20.514(2), c = 12.193(1) \text{ \AA},$ $\beta = 90.49(2)^\circ$
Sperlingite This study	$[(\text{H}_2\text{O})\text{K}](\text{Mn}^{2+}\text{Fe}^{3+})(\text{Al}_2\text{Ti})(\text{PO}_4)_4[\text{O}(\text{OH})](\text{H}_2\text{O})_9(\text{OH})\cdot 4\text{H}_2\text{O}$ $a = 10.428(2), b = 20.281(4), c = 12.223(2) \text{ \AA},$ $\beta = 90.10(3)^\circ$

**Table 2.** Analytical data (wt%) for sperlingite.

	sperlingite			rewitzerite Grey <i>et al.</i> 2023a	
Constituent	Average of 11 analyses				
	Mean	Range	SD		Standard
K <sub>2</sub> O	2.78	2.14-3.65	0.50	3.93	Adularia
MnO	4.56	3.65-5.79	0.72	6.33	MnSiO <sub>3</sub>
MgO	1.42	0.72-2.54	0.64	2.80	Spinel
ZnO	2.51	0.69-4.41	0.93	-	Sphalerite
Al <sub>2</sub> O <sub>3</sub>	5.69	3.32-8.29	1.63	8.37	Berlinite
Fe <sub>2</sub> O <sub>3</sub>	11.77	7.81-14.51	2.22	7.44	Hematite
TiO <sub>2</sub>	11.28	8.79-14.08	1.64	9.18	Rutile
P <sub>2</sub> O <sub>5</sub>	30.21	26.63-32.84	1.76	30.90	Berlinite
F	0.39	0-0.92	0.34	0.87	Fluorite
H <sub>2</sub> O <sub>calc</sub> *	28.74			30.39	
-O≡F	-0.16			-0.37	
Total	99.19			99.84	

\* Based on ideal formula: 14 H<sub>2</sub>O + 2OH<sup>-</sup> per 4P.

**Table 3.** Powder X-ray diffraction data ( $d$  in Å) for sperlingite ( $I_{\text{calc}} > 1.5$ ).

$I_{\text{obs}}$	$d_{\text{obs}}$	$d_{\text{calc}}$	$I_{\text{calc}}$	$hkl$	$I_{\text{obs}}$	$d_{\text{obs}}$	$d_{\text{calc}}$	$I_{\text{calc}}$	$hkl$
37	10.236	10.141	47	0 2 0	11	2.175	2.169	4	-4 4 2
52	7.447	7.383	58	1 1 1			2.159	2	-4 5 1
100	6.176	6.112	100	0 0 2			2.105	2	-2 3 5
		5.277	2	-1 0 2			2.080	2	-2 6 4
		5.214	22	2 0 0	13	2.065	2.064	3	4 6 0
35	5.191	5.147	8	-1 3 1			2.037	8	0 0 6
		5.070	12	0 4 0	8	1.987	1.982	4	4 0 4
		4.675	3	1 2 2			1.957	14	-4 6 2
13	4.704	4.637	7	2 2 0	18	1.961	1.942	5	3 8 2
		3.963	5	2 0 2			1.914	2	-4 7 1
22	3.964	3.910	24	2 3 1	11	1.910	1.890	6	0 4 6
		3.732	4	-1 1 3			1.866	6	-2 2 6
41	3.727	3.697	37	-2 2 2	10	1.869	1.848	5	5 1 3
		3.635	6	2 4 0			1.828	2	-2 8 4
6	3.379	3.380	4	0 6 0	8	1.819	1.805	5	2 10 2
		3.311	3	-1 3 3			1.759	6	-3 0 6
		3.126	2	-2 4 2	6	1.777	1.751	2	-4 7 3
		3.096	46	2 5 1			1.710	3	4 6 4
86	3.101	3.056	20	0 0 4	13	1.695	1.690	9	0 12 0
		3.024	9	-3 0 2			1.676	2	5 7 1
		2.998	2	-3 3 1			1.662	2	-3 4 6
35	2.979	2.958	9	0 6 2	16	1.660	1.654	5	2 6 6
		2.934	14	-1 0 4			1.650	2	-6 2 2
13	2.891	2.894	6	3 2 2			1.644	5	6 4 0
		2.836	24	2 6 0			1.629	2	0 12 2
43	2.839	2.818	8	-1 2 4			1.608	3	2 12 0
		2.772	11	-1 5 3	16	1.602	1.601	3	4 10 0
16	2.648	2.638	4	-2 0 4			1.587	9	-4 2 6
22	2.596	2.594	14	3 4 2	8	1.559	1.548	7	4 10 2
		2.572	10	2 6 2			1.518	3	4 7 5
		2.550	2	2 2 4			1.510	2	6 0 4
11	2.549	2.529	14	4 1 1	8	1.492	1.494	2	-4 11 1
		2.516	2	2 5 3			1.479	3	0 12 4
14	2.492	2.480	9	-2 7 1			1.463	2	0 4 8
		2.461	5	3 3 3	13	1.455	1.449	6	-6 4 4
		2.342	3	0 8 2			1.437	2	0 10 6
10	2.353	2.335	3	-4 2 2			1.417	2	4 3 7
		2.297	4	-3 0 4	6	1.407	1.396	2	2 14 0
10	2.302	2.284	5	1 8 2					



Mineralogical Society

This is a 'preproof' accepted article for Mineralogical Magazine. This version may be subject to change during the production process.

DOI: 10.1180/mgm.2024.40

**Table 4.** Crystal data and structure refinement for sperlingite.

Ideal formula	$(\text{H}_2\text{O})\text{K}(\text{MnFe}^{3+})\text{Al}_2\text{Ti}(\text{PO}_4)_4[(\text{H}_2\text{O})_9(\text{OH})]\cdot 4\text{H}_2\text{O}$
Formula weight	933.6
Symmetry, space group	Monoclinic, $P2_1/c$ (#14)
Unit-cell dimensions	$a = 10.428(2) \text{ \AA}$
	$b = 20.281(4) \text{ \AA}$
	$c = 12.223(2) \text{ \AA}$
	$\beta = 90.10(3)^\circ$
Volume, $Z$	$2585.0(8) \text{ \AA}^3, 4$
Data collection	Synchrotron Microfocus beamline
Wavelength, temperature	$0.7109 \text{ \AA}, 100 \text{ K}$
Crystal size	$0.020 \times 0.020 \times 0.010 \text{ mm}$
Absorption correction	Multiscan, $T_{\min} 0.42, T_{\max} 0.75$
Twinning	2-fold rotation about $c$ . Twin volumes $0.528(3), 0.472(3)$
Theta range for data collect	$1.95 \text{ to } 32.06^\circ$
Index ranges	$-14 \leq h \leq 14, -30 \leq k \leq 30, -16 \leq l \leq 16$
Reflections collected	44006
Independent reflections	7137
Reflections with $I_o > 3\sigma(I)$	5608
Refinement method	Full-matrix least-squares on $F$
Data/constraints/parameters	7122/0/390
Final $R$ indices [ $I > 3\sigma(I)$ ]	$R_{\text{obs}} = 0.050, *wR_{\text{obs}} = 0.058$
$R$ indices (all data)	$R_{\text{obs}} = 0.063, wR_{\text{obs}} = 0.059$
<b>Gooness of Fit</b>	<b>2.80</b>
Largest diff. peak and hole	$1.07 \text{ and } -0.78 \text{ e. \AA}^2$
<b>*<math>w = [\sigma^2( F_o ) + (uF_o)^2]^{-1}</math>, <math>u = \text{instability factor}</math></b>	



**Table 5.** Refined atom coordinates, site scattering (electrons), equivalent isotropic displacement parameters ( $\text{\AA}^2$ ) and bond valence sums (BVS, in valence units) for sperlingite.

Atom	<i>x</i>	<i>y</i>	<i>z</i>	$U_{\text{eq}}$	BVS
M1a	0.49776(7)	0.74704(3)	0.24426(6)	0.0304(2)	2.44
M1b	0.99733(8)	-0.24677(4)	-0.24235(7)	0.0321(3)	2.41
M2a	0.66013(11)	0.50295(4)	0.74325(8)	0.0279(3)	3.56
M2b	1.16103(12)	-0.00360(4)	-0.74169(10)	0.0396(4)	3.65
M3a	0.5	0.5	0.5	0.0293(4)	3.96
M3b	1	0	-0.5	0.0386(5)	4.15
P1a	0.90979(14)	0.59578(5)	0.80203(11)	0.0306(4)	5.08
P1b	1.40937(13)	-0.09537(5)	-0.80165(10)	0.0260(3)	5.07
P2a	0.58744(14)	0.59102(6)	0.29672(10)	0.0264(3)	5.13
P2b	1.08535(14)	-0.09004(6)	-0.29621(12)	0.0304(4)	4.99
A1	0.7222(3)	0.85361(13)	0.0544(2)	0.0401(10)	0.04
A2	1.2241(2)	-0.35214(9)	-0.0565(2)	0.0414(7)	0.48
X1	0.6411(5)	0.50256(14)	0.5980(3)	0.0288(10)	1.64
X2	1.1406(4)	-0.00330(13)	-0.5977(3)	0.0275(9)	1.73
O1a	0.9068(3)	0.67059(13)	0.8053(3)	0.0371(11)	1.80
O1b	1.4026(3)	-0.17065(15)	-0.8047(3)	0.0350(10)	1.74
O2a	1.0286(3)	0.57105(15)	0.7387(3)	0.0312(11)	1.80
O2b	1.5281(3)	-0.07302(14)	-0.7390(3)	0.0311(11)	1.81
O3a	0.9092(4)	0.56747(13)	0.9179(3)	0.0328(11)	1.94
O3b	1.4120(3)	-0.06857(15)	-0.9191(3)	0.0298(10)	1.91
O4a	0.7881(3)	0.57239(16)	0.7440(3)	0.0349(11)	1.87
O4b	1.2866(3)	-0.07183(16)	-0.7445(3)	0.0320(11)	1.96
O5a	0.5967(3)	0.66597(14)	0.2903(3)	0.0332(10)	1.76
O5b	1.0927(3)	-0.16515(14)	-0.2882(3)	0.0383(11)	1.77
O6a	0.4677(3)	0.56553(15)	0.2383(3)	0.0293(10)	1.87
O6b	0.9655(3)	-0.06647(14)	-0.2335(3)	0.0339(11)	1.79
O7a	0.5830(4)	0.56962(15)	0.4157(3)	0.0314(10)	1.96
O7b	1.0822(4)	-0.06751(13)	-0.4163(3)	0.0319(10)	2.03
O8a	0.7080(3)	0.56379(15)	0.2411(3)	0.0297(10)	1.85
O8b	1.2077(4)	-0.06243(15)	-0.2424(3)	0.0374(12)	1.86
O9a	0.3509(4)	0.68932(17)	0.1802(3)	0.0422(12)	0.43
O9b	0.8502(3)	-0.18783(17)	-0.1824(3)	0.0412(12)	0.42
O10a	0.5834(3)	0.74189(17)	0.0852(3)	0.0357(11)	0.37
O10b	1.0803(4)	-0.24262(17)	-0.0820(4)	0.0417(12)	0.45
O11a	0.6437(4)	0.80461(18)	0.3084(4)	0.0459(13)	0.43
O11b	1.1438(3)	-0.30618(16)	-0.3093(3)	0.0384(11)	0.40
O12a	0.4099(3)	0.75085(16)	0.4012(3)	0.0373(11)	0.42
O12b	0.9106(4)	-0.25223(18)	-0.4035(4)	0.0435(13)	0.34
O13a	0.6619(5)	0.50291(15)	0.9133(3)	0.0378(12)	0.40
O13b	1.1642(5)	-0.00345(15)	-0.9125(3)	0.0360(11)	0.39
O14a	0.2636(4)	0.64214(15)	0.4400(3)	0.0456(13)	0.01
O14b	0.7644(3)	-0.14295(15)	-0.4381(3)	0.0429(12)	0.01
O15a	0.5362(3)	0.40625(15)	1.0122(3)	0.0451(8)	0.08
O15b	1.0128(4)	0.0965(3)	-1.0007(3)	0.0708(14)	0.02

**Table 6.** Refined site occupancies and site scattering for sperlingite.

Site	Site scattering used in refinement	Scattering
<i>M1a</i>	0.929(6) Mn* + 0.071 Mg	24.07
<i>M1b</i>	0.801(6) Mn + 0.199 Mg	22.41
<i>M2a</i>	0.31 Fe + 0.40(1) Al + 0.29 Ti	19.64
<i>M2b</i>	0.31 Fe + 0.38(1) Al + 0.31 Ti	19.82
<i>M3a</i>	0.26(1) Al + 0.74 Ti	19.66
<i>M3b</i>	0.23(1) Al + 0.77 Ti	19.93
<i>A1</i>	0.145(8) K + 0.855 O	9.59
<i>A2</i>	0.512(4) K + 0.488 □	9.73

\*Mn scattering curve used for Mn+Fe+Zn

Prepublished Article

**Table 7.** Polyhedral bond lengths [Å] for sperlingite.

<i>M1a</i> - O1b	2.032(3)	<i>M1b</i> - O1a	2.010(3)
-O5a	2.021(3)	-O5b	2.012(3)
-O9a	2.080(4)	-O9b	2.080(3)
-O10a	2.143(4)	-O10b	2.142(5)
-O11a	2.071(4)	-O11b	2.112(4)
-O12a	2.129(4)	-O12b	2.169(4)
Av.	2.079	Av.	2.087
<i>M2a</i> -X1	1.782(3)	<i>M2b</i> -X2	1.772(4)
-O2b	1.991(3)	-O2a	1.958(3)
-O4a	1.940(3)	-O4b	1.905(3)
-O6a	1.939(3)	-O6b	1.963(3)
-O8b	1.913(3)	-O8a	1.932(3)
-O13a	2.079(4)	-O13b	2.088(4)
Av.	1.941	Av.	1.936
<i>M3a</i> -X1 x2	1.897(4)	<i>M3b</i> -X2 x2	1.894(4)
-O3b x2	1.938(3)	-O3a x2	1.942(3)
-O7a x2	1.951(3)	-O7b x2	1.912(3)
Av.	1.929	Av.	1.916
<i>P1a</i> -O1a	1.518(3)	<i>P1b</i> -O1b	1.529(3)
-O2a	1.545(4)	-O2b	1.523(4)
-O3a	1.528(4)	-O3b	1.535(3)
-O4a	1.528(4)	-O4b	1.536(3)
Av.	1.530	Av.	1.531
<i>P2a</i> -O5a	1.525(3)	<i>P2b</i> -O5b	1.528(3)
-O6a	1.527(3)	-O6b	1.541(4)
-O7a	1.518(3)	-O7b	1.538(4)
-O8a	1.533(4)	-O8b	1.540(4)
Av.	1.526	Av.	1.537
<i>A1</i> -X1	3.084(4)	<i>A2</i> -X2	3.099(3)
-O4a	2.845(5)	-O4b	2.844(4)
-O7a	2.720(4)	-O7b	2.791(4)
-O9b	3.297(5)	-O9a	3.288(5)
-O10a	2.715(4)	-O10b	2.698(4)
-O11a	3.363(5)	-O11b	3.333(5)
-O12b	2.890(4)	-O12a	2.871(4)
-O15b	3.016(6)	-O15a	2.781(5)
Av.	2.991	Av.	2.963

**Table 8.** H-bonding in sperlingite.

Donor..Acceptor	O..O (Å)	Bond valence*
O9a..O5b	2.764	0.198
O9a..O6a	2.879	0.158
O9a..O1b	2.896	0.154
O9b..O5a	2.7	0.227
O9b..O6b	2.81	0.180
O10a..O12a	2.887	0.156
O10a..O14b	2.77	0.195
O10b..O12b	2.814	0.179
O10b..O14a	2.807	0.181
O11a..O1a	2.79	0.187
O11a..O4a	3.019	0.127
O11a..O2b	2.819	0.177
O11b..O1b	2.739	0.208
O11b..O2a	2.827	0.174
O11b..O4b	2.993	0.132
O12a..O14a	2.723	0.215
O12b..O14b	2.723	0.215
O12b..A1	2.89	0.155
O13a..O15a	2.651	0.254
O13a..X2	3.053	0.121
O13a..O3a	2.893	0.155
O13a..O7b	3.027	0.125
O13b..X1	3.049	0.122
O13b..O3b	2.903	0.152
O13b..O7a	3.024	0.126
O13b..O15b	2.785	0.189
O14a..O3b	2.753	0.202
O14a..O8b	2.814	0.179
O14a..O12a	2.723	0.215
O14b..O8a	2.779	0.192
O14b..O3a	2.781	0.191
O15a..O2b	2.884	0.157
O15b..O14a	3.118	0.111
O15b..A1	3.016	0.127
A1..O7a	2.720	0.217
A1-O15b	3.016	0.127

\*from Ferraris, G. and Ivaldi, G. (1988).

**Table 9.** Comparison of rewitzerite and sperlingite.

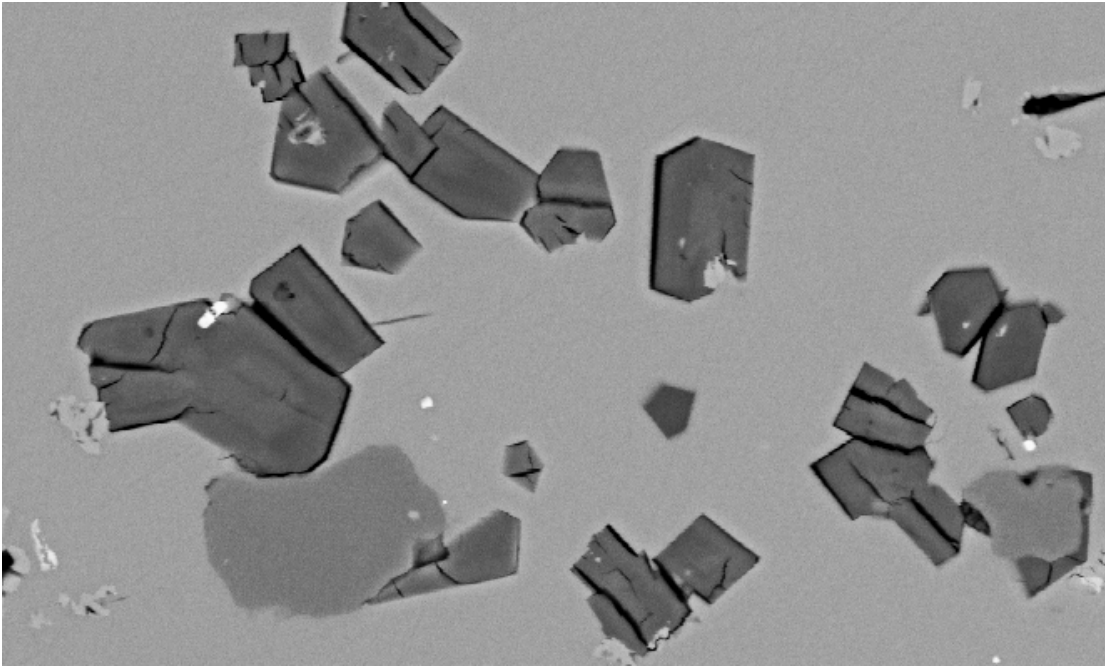
	rewitzerite	sperlingite
Ideal Formula	$\text{K}(\text{H}_2\text{O})\text{Mn}_2(\text{Al}_2\text{Ti})(\text{PO}_4)_4[\text{O}(\text{OH})]$ $(\text{H}_2\text{O})_{10} \cdot 4\text{H}_2\text{O}$	$(\text{H}_2\text{O})\text{K}(\text{Mn}^{2+}\text{Fe}^{3+})(\text{Al}_2\text{Ti})(\text{PO}_4)_4[\text{O}(\text{OH})]$ $[(\text{H}_2\text{O})_9(\text{OH})] \cdot 4\text{H}_2\text{O}$
Crystal System	monoclinic	
Space Group	$P2_1/c$	
$a$ (Å)	10.444(2)	10.428(2)
$b$ (Å)	20.445(2)	20.281(4)
$c$ (Å)	12.2690(12)	12.223(2)
$\beta$ (°)	90.17(3)	90.10(3)
$V$ (Å <sup>3</sup> )	2619.8(6)	2585.0(8)
$Z$	4	
Strongest	10.26 (53) (020)	10.236 (37) (020)
lines in	7.44 (55) (-111)	7.447 (5) (111)
X-ray	6.16 (92) (002)	6.176 (100) (002)
powder	5.19 (40) (200)	5.191 (35) (200)
pattern	3.958 (32) (-231)	3.964 (22) (231)
$D$ (I) ( $hkl$ )	3.703 (57) (-222)	3.727 (41) (-222)
	3.111 (97) (-251)	3.101 (86) (251)
	2.862 (100) (260)	2.839 (43) (260)
Dcalc (g·cm <sup>-3</sup> )	2.33	2.40
Opt. Character	biaxial (+)	biaxial (+)
$\alpha$	1.585(2)	1.600(est.)
$\beta$	1.586(2)	1.615(5)
$\gamma$	1.615(2)	1.635(5)
$2V_{\text{meas}}$ (°)	25(2)	82.7 (calc.)
Reference	Grey et al. (2023c)	This study



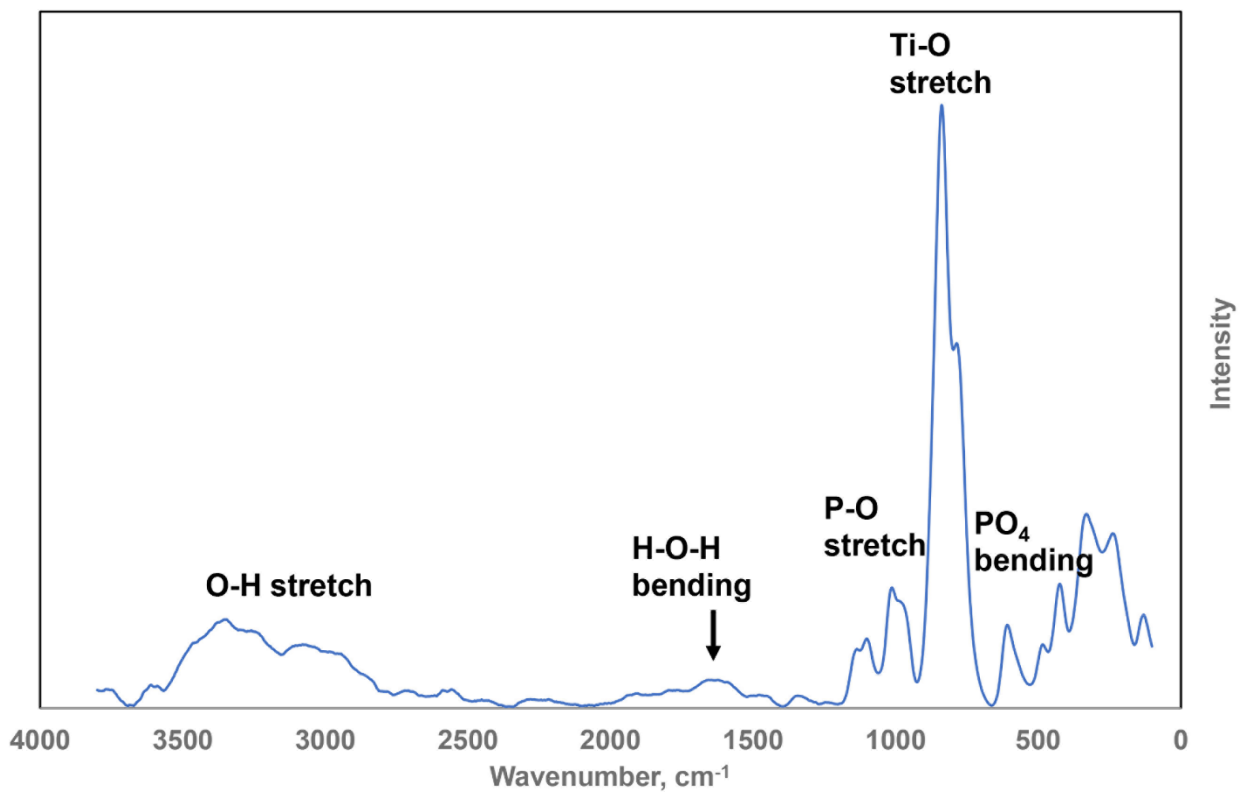
Figure 1. Aggregates of colourless sperlingite crystals in corrosion pit in zwieselite associated with scholzite (large crystal in upper left). Photo by Christian Rewitzer, [holotype specimen MSM38185](#), FOV = 0.3 mm.



Figure 2. Aggregates of sperlingite crystals associated with sprays of zincoberaunite needles. Brown staining on sperlingite is mitridatite. Photo by Christian Rewitzer, **holotype specimen MSM38185**.



**Figure 3.** Back-scattered electron image of polished epoxy mount of holotype specimen **MSM38185**, used for EMP analyses, showing dark grey sperlingite crystals in a light grey scholzite matrix, associated with fluor-apatite (medium grey). FOV = 80  $\mu\text{m}$ .



**Figure 4.** Raman spectrum of sperlingite.



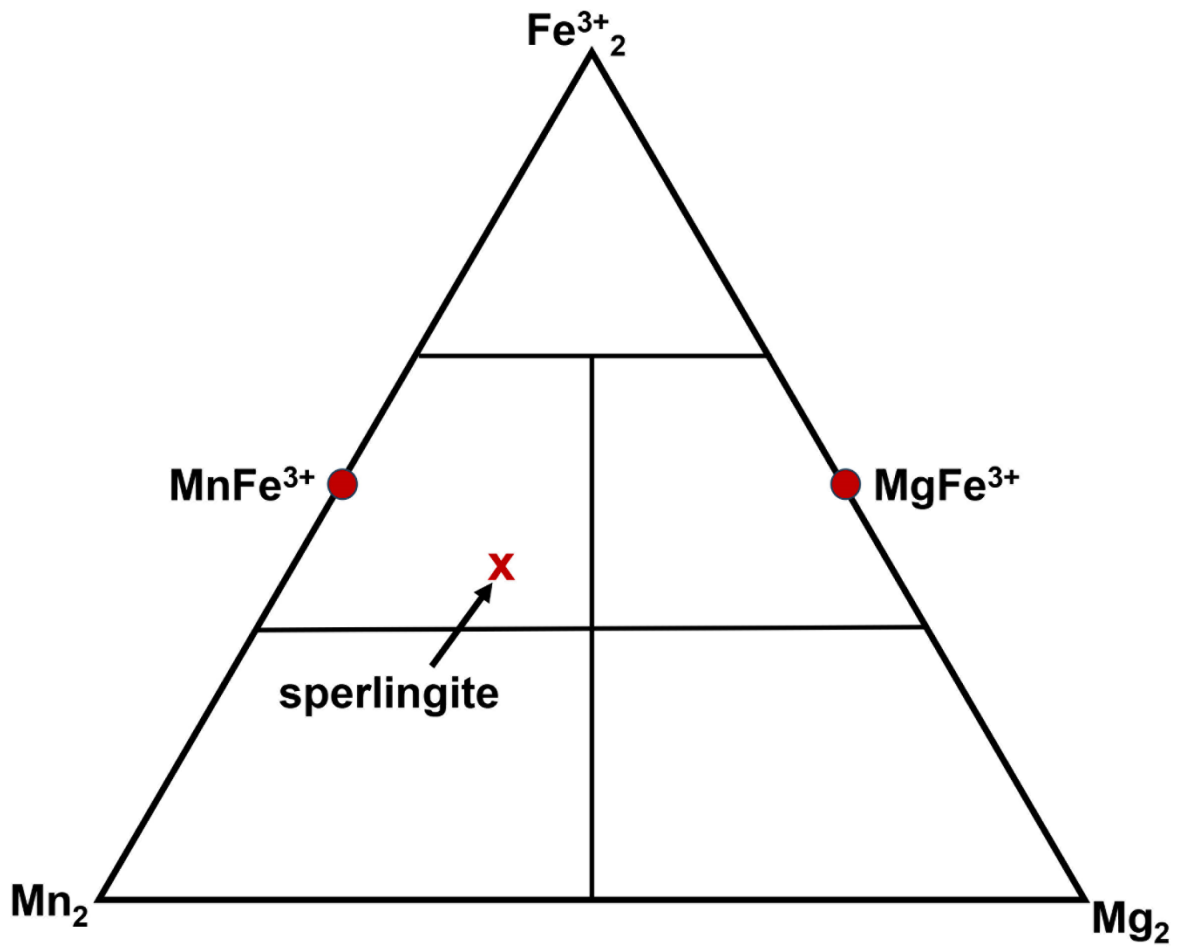


**Figure 5.** ternary diagram for (M1)<sub>2</sub> site Mn<sup>2+</sup>-Mg-Fe<sup>3+</sup> compositions, showing end-member compositions and location of the empirical composition for sperlingite. Note that the divalent cations correspond to the dominant cations found at M1 in paulkerrite-group minerals.

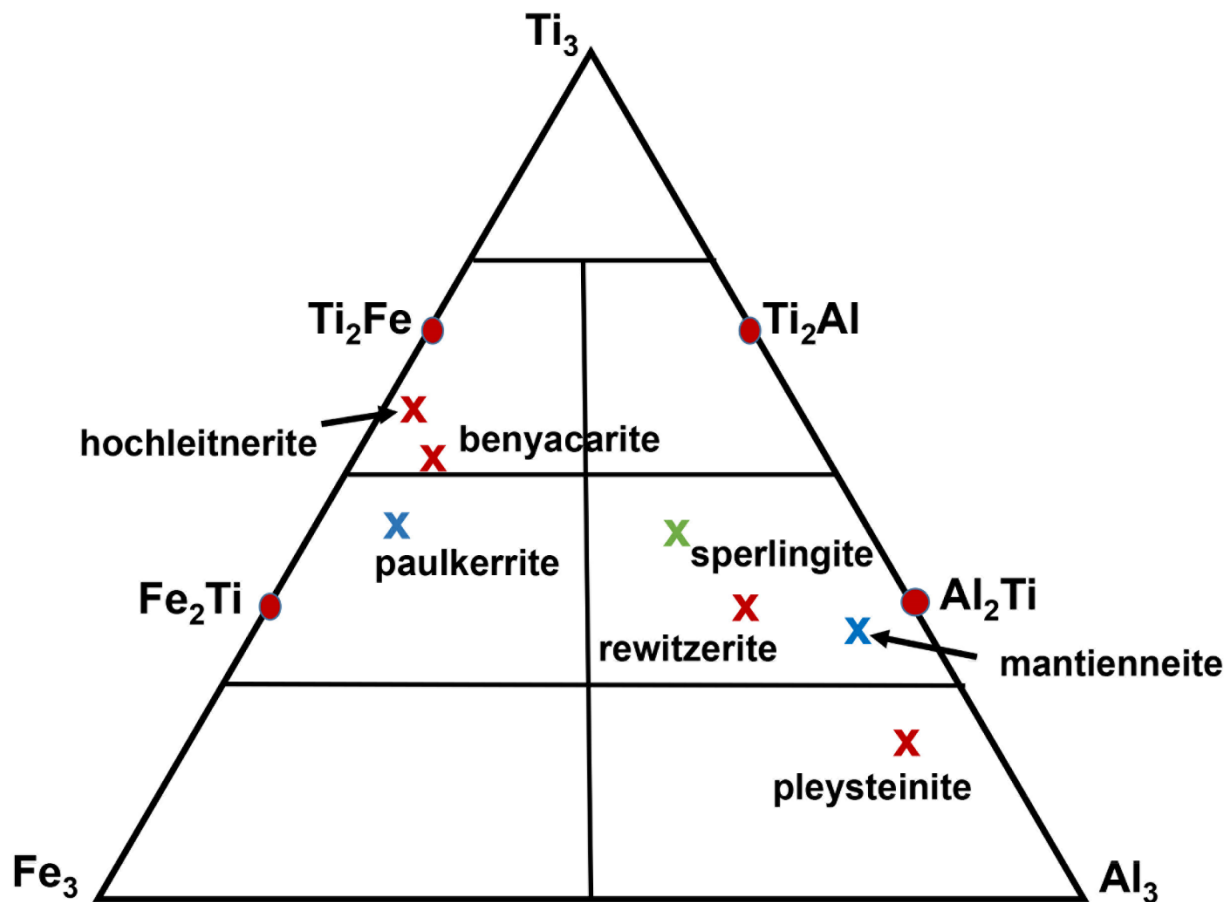


**Figure 6.** Ternary diagram for  $(M2)_2M3$  site Al-Ti-Fe<sup>3+</sup> compositions, showing end-member compositions (Al<sub>2</sub>Ti, Ti<sub>2</sub>Al etc.) and location of the empirical composition for sperlingite. For comparison the published empirical compositions are shown for the paulkerrite-group minerals benyacarite (Demartin *et al.*, 1993,1997), paulkerrite (Peacor *et al.*, 1984), mantienneite (Fransolet *et al.*, 1984), rewitzerite (Grey *et al.*, 2023a), pleysteinite (Grey *et al.*, 2023c) and hochleitnerite (Grey *et al.*, 2023d). Red crosses correspond to minerals with Mn at *M1* and blue crosses correspond to minerals with Mg at *M1*.

